Chinese Chemical Letters 33 (2022) 4776–4780

Contents lists available at ScienceDirect

Chinese Chemical Letters

journal homepage: www.elsevier.com/locate/cclet

Electrochemical reaction mechanism of porous $Zn_2Ti_3O_8$ as a high-performance pseudocapacitive anode for Li-ion batteries

Weijie Cheng[a], Qi Feng[a,c,*], Zhanglin Guo[b], Guanjun Chen[a], Yong Wang[a], Lixiong Yin[a], Jiayin Li[a], Xingang Kong[a,*]

[a] School of Materials Science and Engineering, Shaanxi University of Science and Technology, Xi'an 710021, China
[b] Graduate School of Engineering, Toin University of Yokohama, Kanagawa 225-8503, Japan
[c] Department of Advanced Materials Science, Faculty of Engineering, Kagawa University, 2217-20 Hayashi-cho, Takamatsu-shi 761-0396, Japan

ARTICLE INFO

Article history:
Received 29 September 2021
Revised 9 December 2021
Accepted 4 January 2022
Available online 8 January 2022

Keywords:
$Zn_2Ti_3O_8$
Lithium-ion battery
Electrochemical reaction mechanism
Theoretical capacity
Pseudocapacitance

ABSTRACT

$Zn_2Ti_3O_8$, as a new type of anode material for lithium-ion batteries, is attracting enormous attention because of its low cost and excellent safety. Though decent capacities have been reported, the electrochemical reaction mechanism of $Zn_2Ti_3O_8$ has rarely been studied. In this work, a porous $Zn_2Ti_3O_8$ anode with considerably high capacity (421 mAh/g at 100 mA/g and 209 mAh/g at 5000 mA/g after 1500 cycles) was reported, which is even higher than ever reported titanium-based anodes materials including $Li_4Ti_5O_{12}$, TiO_2 and $Li_2ZnTi_3O_8$. Here, for the first time, the accurate theoretical capacity of $Zn_2Ti_3O_8$ was confirmed to be 266.4 mAh/g. It was also found that both intercalation reaction and pseudocapacitance contribute to the actual capacity of $Zn_2Ti_3O_8$, making it possibly higher than the theoretical value. Most importantly, the porous structure of $Zn_2Ti_3O_8$ not only promotes the intercalation reaction, but also induces high pseudocapacitance capacity (225.4 mAh/g), which boosts the reversible capacity. Therefore, it is the outstanding pseudocapacitance capacity of porous $Zn_2Ti_3O_8$ that accounts for high actual capacity exceeding the theoretical one. This work elucidates the superiorities of porous structure and provides an example in designing high-performance electrodes for lithium-ion batteries.

As a kind of clean energy, the application of lithium ion battery (LIBs) is becoming more and more common in our lives, especially in these areas of pure electric vehicles, now-ubiquitous man-carried electronics and smart grids [1,2]. It is urgent to develop LIBs with high reversible capacity, great long-cycle stability and excellent performance at large current density [3]. Recently, it has been found that the introduction of pseudocapacitive charge storage into LIBs is an effective way to fabricate ultra-fast charging-discharging rate LIBs. Thanks to the synergy between the battery reaction and pseudocapacitance, it can ensure high rate performance and bring additional capacity [4]. Meanwhile, the behavior of pseudocapacitance was generally presented in materials with porous structures and nanomaterials [5–8].

Traditional Ti-based anode materials for LIBs, such as $Li_4Ti_5O_{12}$, TiO_2 and $Li_2ZnTi_3O_8$ as typical intercalation type anodes materials have caught much attention thanks to their cheap manufacturing costs, good sustainability, environment protecting, and good safety [9–13]. Recently, $Zn_2Ti_3O_8$ a new Ti-based material with cubic defect spinel structure, has entered the field of view of scholars when used as anode material for LIBs. Its electrochemical properties were first reported by Hong *et al.* in 2010 [14], and the capacity of $Zn_2Ti_3O_8$ nanowires reached to about 400 mAh/g at 100 mA/g, which is much higher than that of these traditional Ti-based materials just like $Li_4Ti_5O_{12}$ (175 mAh/g), TiO_2 (335 mAh/g), $Li_2ZnTi_3O_8$ (227 mAh/g) and $MLi_2Ti_6O_{14}$ (about 240 mAh/g). However, up to now, there are only few literatures on the electrochemical properties of $Zn_2Ti_3O_8$ and its electrochemical reaction mechanism is only speculated according to its capacity voltage curves and volt-ampere cycle curves. Liao *et al.* deemed that both Ti and Zn were involved in the electrochemical reaction [15,16]. While Wang *et al.* believed that only Ti was involved in the electrochemical reaction during charging-discharging [17]. Therefore, besides achieving high performance, it is necessary to study on electrochemical reaction mechanism that accounts for high performance.

Recently, we have reported the porous network $Zn_2Ti_3O_8$ plate-like nanoarchitecture [18] *via* the *in situ* topotactic reaction of layered $H_{1.07}Ti_{1.73}O_4{\cdot}H_2O$ precursor [19–21], and deeply researched its formation mechanism. The preliminary study of electrochemical properties indicated that such porous network $Zn_2Ti_3O_8$

* Corresponding authors.
E-mail addresses: feng@eng.kagawa-u.ac.jp (Q. Feng), yezhu_1983@163.com (X. Kong).

https://doi.org/10.1016/j.cclet.2022.01.002
1001-8417/

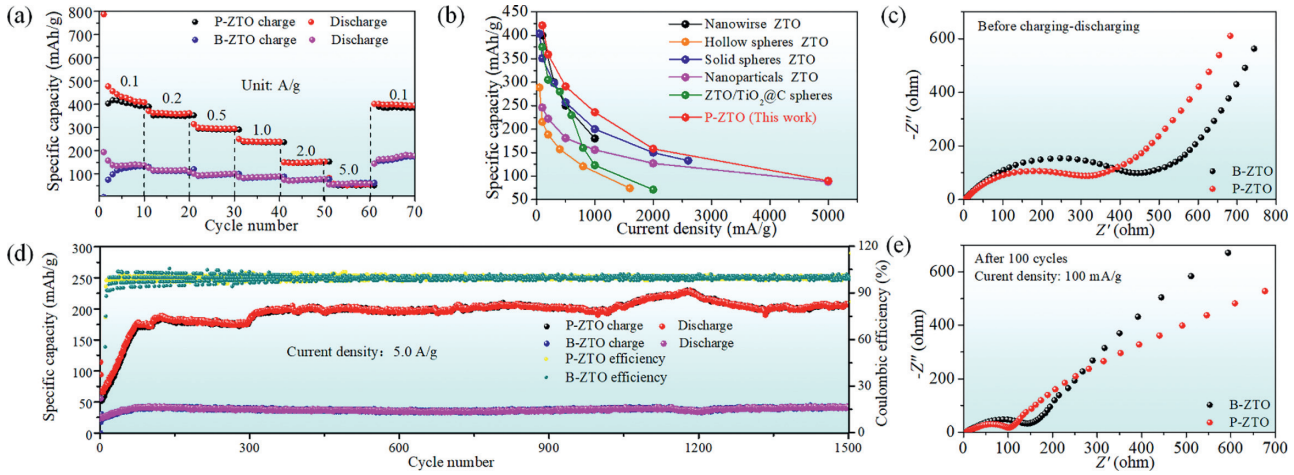

Fig. 1. Rate performance (a) of P-ZTO and B-ZTO. (b) Performance comparison with other $Zn_2Ti_3O_8$ (ZTO) reported in recent years [14-17,22]. (d) Long cycle performance of P-ZTO and B-ZTO. EIS analysis of two samples before charging-discharging (c) and after 100 cycles at 100 mA/g (e).

platelike particles presented a high specific capacity (421 mAh/g at 100 mA/g), and its reversible capacity still remained 209 mAh/g at 5000 mA/g during 1500 cycles, which greatly exceeded that of the commercial $Li_4Ti_5O_{12}$ anodes material. Though the high performance was achieved, the reasons and mechanism were barely discussed and still unclear. In this paper, we further studied the electrochemical reaction mechanism of porous $Zn_2Ti_3O_8$ particles. For the first time, we accurately confirmed its electrochemical reaction equation and calculated its theoretical intercalation capacity *via* first-principles (Some scholars believe that the theoretical capacity of $Zn_2Ti_3O_8$ is 466 mAh/g, but no evidences are available. As we calculate here, the accurate theoretical capacity of $Zn_2Ti_3O_8$ should be 266.4 mAh/g rather than 466 mAh/g). For the phenomenon that its actual capacity exceeds the theoretical intercalation capacity, it is confirmed that it is due to the generation of a large number of pseudocapacitance behavior in the charging-discharging process. Meanwhile, through the analysis of the correlation between morphology and electrochemical performance, we found that the porous structure not only brings much pseudocapacitance capacity but also promotes its intercalation reaction. So, the porous $Zn_2Ti_3O_8$ has a better rate performance and higher reversible capacity due to the synergistic effect of pseudocapacitance and enhanced intercalation reaction. The experimental details are shown in Supporting information.

The sample preparation flowchart is shown in Fig. S1 (Supporting information). To highlight the advantages of porous $Zn_2Ti_3O_8$ (P-ZTO), the $Zn_2Ti_3O_8$ bulk sample (B-ZTO) was selected as a comparison. The XRD patterns of two $Zn_2Ti_3O_8$ samples prepared by different methods are shown in Fig. S2a (Supporting information), where both samples show pure $Zn_2Ti_3O_8$ phase (JCPDS No. 87–1781). While big difference in morphology can be observed in SEM and TEM images. The sample prepared by the ion-exchange method shows a plate-like morphology with evenly distributed mesoporous on the surface (Figs. S2b and d in Supporting information). On the other hand, the reference sample prepared by the molten salt method (B-ZTO) consists of bulks (Figs. S2c and e in Supporting information). More characterization information of P-ZTO and B-ZTO was shown in Fig. S3 (Supporting information). In the SEM image of P-ZTO (Fig. S3a), it can be observed that its thickness is about 20 nm. In the TEM photographs of P-ZTO (Figs. S3b-d), there are a particularly large number of evenly distributed holes. The Brunauer-Emmett-Teller (BET) analysis of the two samples showed that the specific surface area of P-ZTO was 40.6 m^2/g, which was much larger than that of B-ZTO (6.7 m^2/g). Meanwhile, the result showed that the pore size of P-ZTO was about 10 nm (Figs. S3e and f).

Fig. 1 shows the electrochemical performance of electrodes fabricated using P-ZTO and B-ZTO. In the rate performance test, the P-ZTO has a higher reversible capacity than that of B-ZTO at the same current densities from 100 mA/g to 5000 mA/g. Particularly, at current density of 100 mA/g, the reversible capacity of the P-ZTO can reach to 421 mAh/g, while only 140 mAh/g for that of B-ZTO (Fig. 1a). We compared our high-capacity results with those of previous reports. As summarized in Fig. 1b, one can find that the capacities achieved for P-ZTO under different current densities are higher than ever-reported values [14-17,22], proving the advantage of the mesoporous structure of P-ZTO.

Moreover, as shown in Fig. 1d, in the long-term cycle process at the high current density of 5000 mA/g, although the coulombic efficiencies are quite similar, the capacity of P-ZTO is stable to be 209 mAh/g after 1500 cycles, which is much higher than that of B-ZTO sample (50 mAh/g). What is more, the EIS analysis are shown in Figs. 1c and e. The result shows that the electrolyte resistance of two samples is similar, while P-ZTO has significantly lower charge transfer resistance than that of B-ZTO [23]. Since the gap between particles is an important factor affecting the charge transfer resistance, we analyzed that the lower impedance of P-ZTO is due to its special porous plate structure. The charge can be rapidly transmitted on the flat surface of the P-ZTO. While as B-ZTO is composed of bulks, there is a large gap between each bulk, which is not conducive to charge transmission. These results indicate that besides the high capacity, P-ZTO also possesses high cycle stability at high current density, manifesting its potential for practical application, especially in quick charge for electric vehicles.

Fig. S4a (Supporting information) presents the capacity voltage curve of P-ZTO. The discharge capacity in the first turn reaches 700 mAh/g, but attenuates to 450 mAh/g in the second cycle. This phenomenon can be attributed to the formation of solid electrolyte interface (SEI) layer on the electrode surface during the first charge-discharge, resulting in part of consumption of Li^+ ions and the irreversible capacity loss. This phenomenon occurs in most anode materials [24]. As the charge-discharge continues, the reversible capacity of electrode material gradually reached 421 mAh/g and remained stable. At the same time, it can be observed that there are two platforms around 0.5 V and 1.5 V, respectively. In the volt-ampere cycle curves (Fig. S4b in Supporting information), the first lap also exhibits a remarkable difference compared with the second lap and third lap. The cathode peak at 0.6 V in the first

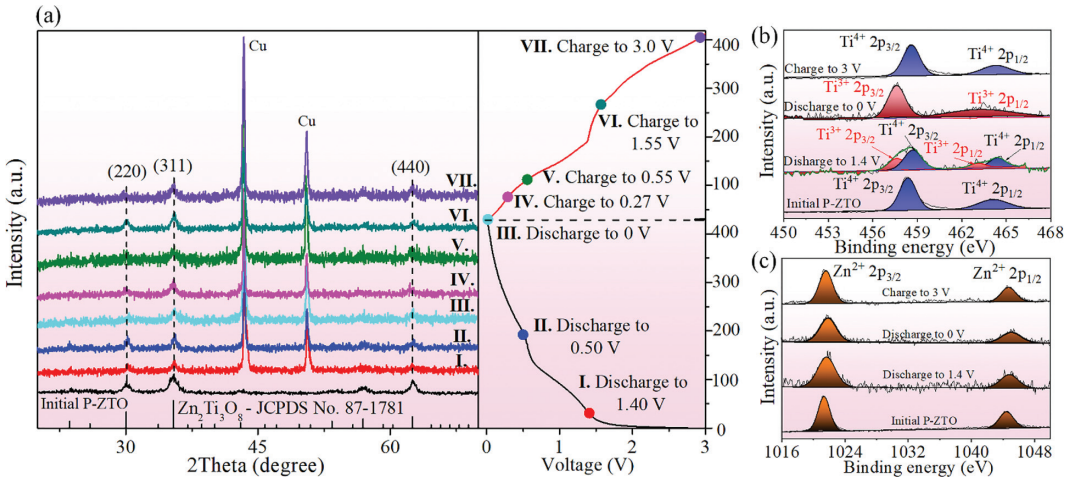

Fig. 2. (a) XRD pattern of the P-ZTO at the different charging-discharging stages. The XPS spectra of Ti (b) and Zn (c) elements at different charging-discharging stages of P-ZTO.

cycle was caused by SEI, which is not observed in the subsequent volt-ampments cycle. In the second and third cycle curves, two groups of redox peaks at 1.55/1.4 V and 0.5/0.27 V can be assigned to the evolution of Ti^{4+}/Ti^{3+} during charging and discharging [25]. The capacity voltage curves and volt-ampere cycle curves of B-ZTO show the similar phenomenon as discussed above (Figs. S4c and d in Supporting information).

For better understanding the high capacity and high stability of P-ZTO, as the prime target of this work, the electrochemical reaction mechanism was studied. Firstly, the structure and morphology evolution of P-ZTO during the charging-discharging process were investigated. The half-cells were activated *via* 100 cycles of charging-discharging, and then disassembled at the specific potentials corresponding to the redox peaks in the voltametric cycle. In general, for electrode materials of LIBs, obvious changes in morphology and volume occur during the conversion or alloying reaction [26,27], while not for intercalation reaction [28]. The SEM images (Fig. S5 in Supporting information) display that P-ZTO electrode materials at different electrochemical reaction stages remained the pristine platelike morphology, which suggests that the battery reaction of P-ZTO should be only intercalation reaction. And to confirm this, the XRD test was carried out at seven different charging-discharging stages according to the capacity voltage curve shown on the right (Fig. 2a). The diffraction peaks at 43.4° and 50.7° are assigned to copper foil used for electrode assembling. It's clear that all the samples from different stages still remain the pure $Zn_2Ti_3O_8$ phase. This result confirms that there is no phase transformation during charging and discharging process, which also excludes the possibility of conversion reaction and alloying reaction, agreeing well with the above SEM results. For further understanding the electrochemical reaction mechanism, the above samples were characterized by XPS (Fig. S6 in Supporting information) and the spectra of Ti and Zn elements of P-ZTO at different charging-discharging stages are shown in Figs. 2b and c. The initial Ti 2p XPS spectrum shows two peaks at 458.3 eV and 464.3 eV, corresponding to Ti^{4+} $2p_{3/2}$ and Ti^{4+} $2p_{1/2}$, respectively. When the P-ZTO electrode discharged from 3 V to 1.4 V after 100 cycles, the Ti 2p peaks can be fitted to four peaks. The peaks at 457.6 eV and 463.0 eV should be attributed to Ti^{3+} $2p_{3/2}$ and Ti^{3+} $2p_{1/2}$, and the peaks at 458.3 eV and 464.3 eV are corresponding to Ti^{4+} $2p_{3/2}$ and Ti^{4+} $2p_{1/2}$, identifying the co-existence of Ti^{3+} and Ti^{4+} at this stage. Continuing to discharge to 0 V, the curve can be fitted to only two peaks located at 457.6 eV and 463.0 eV, which means the Ti^{4+} is fully reduced to Ti^{3+}. When the electrode

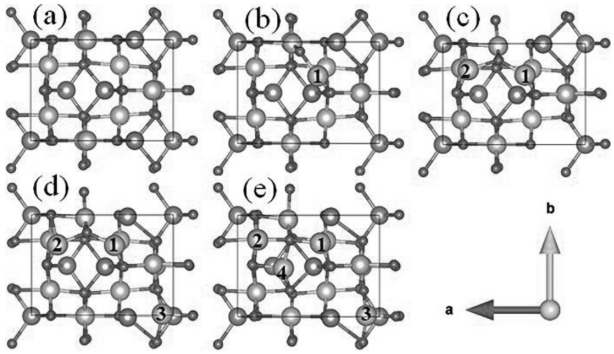

Fig. 3. Ground-state structures of $xZn_2Ti_3O_8$ with x = 0, 1, 2, 3 and 4 from (a) to (e). (Green ball: Li, red ball: O, blue ball: Ti, gray ball: Zn).

charged to 3 V from 0 V, the binding energy of Ti 2p returned back to 458.3 eV and 464.3 eV, corresponding to Ti^{4+} $2p_{3/2}$ and Ti^{4+} $2p_{1/2}$ respectively, which implies the Ti^{3+} are oxidized to Ti^{4+} ions [25]. However, under the different charging-discharging stages, the Zn 2p XPS spectra remain the same and two peaks at 1021 eV and 1044 eV belonging to Zn^{2+} $2p_{3/2}$ and Zn^{2+} $2p_{1/2}$, respectively. The constant valence indicates that zinc ions are not involved in the redox reactions and only titanium ions work in the charging-discharging process.

Based on the above results, it's sure that the battery reaction in P-ZTO electrode material is pure intercalation reaction, the same with that of $Li_4Ti_5O_{12}$, as previously reported [29]. The intercalation reaction can be written as Eq. 1:

$$Zn_2Ti_3O_8 + xLi^+ + xe^- \rightarrow Li_xZn_2Ti_3O_8 \quad (1)$$

Though the high capacity was achieved and the electrochemical reaction mechanism was elucidated here, the study on $Zn_2Ti_3O_8$ materials is still insufficient. For example, the theoretical specific capacity is still unknown. Therefore, here for the first time, we calculated the theoretical specific capacity with the help of first-principles DFT calculations [30–33], as shown in Fig. 3. It is found that the maximum number of inserted Li^+ in the unit cell is 4. Once we have determined its reaction formula and the maximum number of inserted Li^+, we can calculate its theoretical capacity according to Eq. 2 [34]:

$$C = mF/3.6M \quad (2)$$

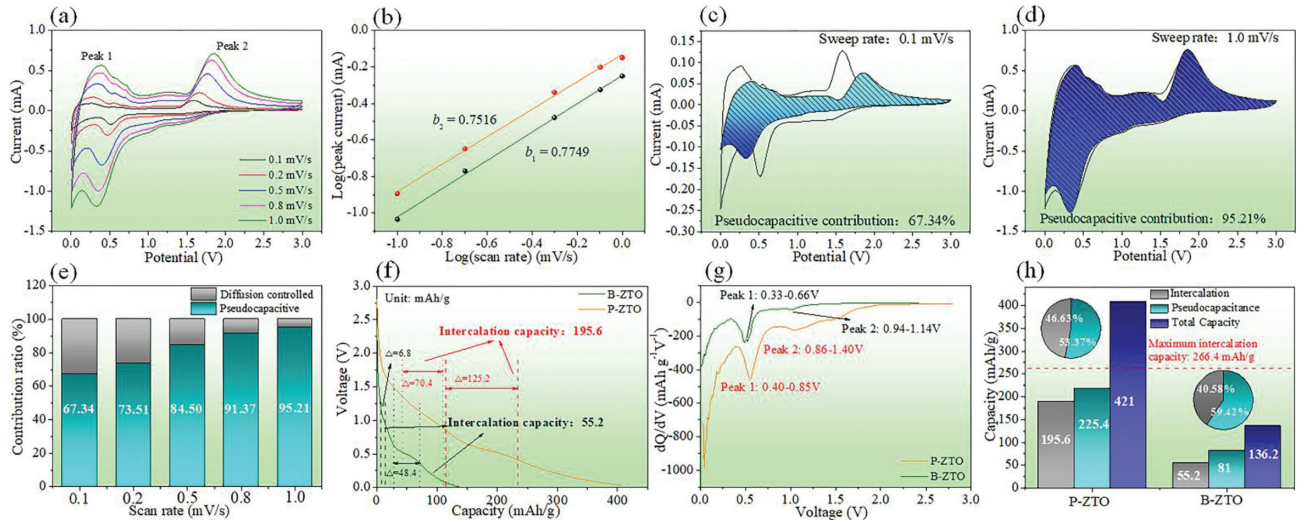

Fig. 4. Cyclic voltammetry of P-ZTO at different scan rates (a) and corresponding peak current *versus* square root of scan rates (b). Pseudocapacitance contribution ratio of P-ZTO at scan rates of 0.1 mV/s (c), 1.0 mV/s (d) and their summary histogram (e). Capacity voltage curve and intercalation capacity calculation at 100 mA/g of two ZTO (f). The dQ/dV curve analysis of two ZTO (g). Total capacity and capacity contribution of each lithium storage behavior (h).

where C is the specific capacity (mAh/g), m is the number of Li atoms in the final discharge product, F is the Faraday constant (96,485 C/mol), and M is the mole weight of $Zn_2Ti_3O_8$ (402.43 g/mol). The theoretical specific capacity of $Zn_2Ti_3O_8$ electrode is calculated to be 266.4 mAh/g. It is quite interesting that the actual capacity achieved (421 mAh/g) in our experiment is much higher than that from theoretical specific capacity.

It has been proved that the porous materials, when working as electrodes, are prone to generate pseudocapacitance, which contributes to a significant increase in electrode material capacity [35–37] and this may explain the observation in our study. To confirm the existence of the pseudocapacitance behavior in our P-ZTO electrode, volt-ampere cycle texts at different sweeping speeds were carry out and the results are shown in Fig. 4a. According to the peak current and sweeping speed, we do the linear fitting *via* Eq. 3 [38]:

$$I = a * v^b \tag{3}$$

where i is the peak current, v is the sweeping speed, and a and b are adjustable parameters. When b value is 0.5, it is indicated that Li^+ intercalation process is the dominant process. When the value of b is close to 1, it is suggested that the reaction mainly comes from the surface capacitance effect, namely pseudocapacitance. After linear fitting, as shown in Fig. 4b, we calculated $b_1 = 0.77$ and $b_2 = 0.75$ at two lithium intercalation stages (0.27 V and 1.5 V) respectively. These results imply that the pseudocapacitance and intercalation reaction act together in charging-discharging processes.

Through the analysis of volt-ampere-cycle measurements at different rates, the pseudocapacitance contribution can be quantified. Using the above concepts, the current response at fixed potential can be expressed as shown in Eq. 4 [39]:

$$i(V) = k_1 v + k_2 v^{1/2} \tag{4}$$

$k_1 v$ and $k_2 v^{1/2}$ correspond to the current contribution of surface capacitance effect and intercalation process, respectively. To simplify the calculation process, Eq. 4 can be translated into Eq. 5:

$$i(V)/v^{1/2} = k_1 v^{1/2} + k_2 \tag{5}$$

At a certain potential, the current value was measured under each scan rate. A plot of $i/v^{1/2}$ *versus* $v^{1/2}$ allowed the calculation of k_2 from the y-intercept, and k_1 from the slope of Eq. 5. Thus, by determining k_1 and k_2, we can quantify the pseudocapacitance contribution at different working currents [40,41]. By the integral calculation, we obtained the percentage of pseudocapacitance contribution for P-ZTO at different scan rates. At a low sweep rate of 0.1 mV/s, the pseudocapacitance contribution reaches up to 67.34% (Fig. 4c), and it is clear that with the working current increasing, the proportion of pseudocapacitance increases and finally becomes dominant in the total capacity (95.21%), which must be the reason for the excellent rate performance of P-ZTO [42] (Fig. 4d). Its pseudocapacitance contribution at different scan rates can be found in the summary histogram, and they are 67.34%, 73.51%, 84.5%, 91.37% and 95.21% at 0.1, 0.2, 0.5, 0.8 and 1.0 mV/s, respectively (Fig. 4e). In this work, the P-ZTO anode not only shows a much higher capacity than that of B-ZTO, but also a better performance than other popular Ti-base anode materials under high current density as well as higher contribution proportions of pseudocapacitance (summarized in Table S1 in Supporting information) [43–46]. Besides, the same pseudocapacitance tests for the B-ZTO are shown in Figs. S7 and S8 (Supporting information). To our surprise, B-ZTO also has a large amount of pseudocapacitance behavior. Therefore, other analyses will be conducted to explore why P-ZTO has a higher capacity than ZTO of other morphologies.

In order to highlight the performance advantages brought by its porous structure, we quantified the capacity contribution of each reaction [47,48] of P-ZTO and B-ZTO. After 100 stable cycles at 100 mA/g, the reversible capacity of P-ZTO and B-ZTO are 421 mAh/g and 136 mAh/g, respectively (Fig. 4f). Fig. 4g is the dQ/dV curve obtained from the capacity voltage curves in Fig. 4f. The peaks of 0.40–0.85 V and 0.86–1.40 V represent the two stages of intercalation for P-ZTO, while the B-ZTO intercalation occur at 0.33–0.66 V and 0.94–1.14 V. According to our calculation, the intercalation capacities of P-ZTO and B-ZTO are 195.6 mAh/g and 55.2 mAh/g, respectively, reaching 86.39% and 20.72% of the theoretical intercalation capacity (266.4 mAh/g). At the same time, the pseudocapacitance capacities of P-ZTO and B-ZTO are 225.4 mAh/g and 81 mAh/g, respectively, accounting for 53.56% (P-ZTO: 421 mAh/g) and 59.55% (B-ZTO: 136 mAh/g) of their reversible capacity (Fig. 4h). In other words, although B-ZTO has a large proportion of pseudocapacitance, the contribution value of pseudocapacitance and intercalation capacity is too small, which leads to the performance of B-ZTO is far inferior to that of P-ZTO.

On one hand, the mesoporous provide rapid channels for lithium ions to pass through, enhancing the intercalation reaction. On the other hand, they also provide more attachment sites to adsorb lithium ions [49], resulting in increased surface capacitance contribution (pseudocapacitance). While these advantages are not observable in B-ZTO and other Ti-based materials without such a porous structure. It is believed that P-ZTO has the potential to work as a new type pseudocapacitive lithium-ion anodes electrode material. Moreover, the elucidated electrochemical reaction mechanism will provide ideas in designing more highly efficient porous electrode materials.

In summary, we reported a high-performance porous $Zn_2Ti_3O_8$ anode for lithium-ion batteries and deeply studied the electrochemical reaction mechanism. The porous $Zn_2Ti_3O_8$ anode showed a capacity of 421 mAh/g at 100 mA/g, the highest value for the reported $Zn_2Ti_3O_8$-based anodes, while only 140 mAh/g for bulk $Zn_2Ti_3O_8$. Moreover, the porous $Zn_2Ti_3O_8$ kept a capacity of 209 mAh/g at 5000 mA/g after 1500 cycles, indicating its outstanding cycling stability. For studying the mechanism of the high performance of the porous $Zn_2Ti_3O_8$, we calculated the theoretical capacity of $Zn_2Ti_3O_8$ by DFT calculation, showing 266.4 mAh/g, lower than the achieved actual capacity. With comprehensive characterizations, we confirmed that both intercalation reaction and pseudocapacitance contribute to the capacity of $Zn_2Ti_3O_8$. The designed porous structure of $Zn_2Ti_3O_8$ not only promotes the intercalation reaction, but also induces high pseudocapacitance capacity of 225.4 mAh/g, boosting the reversible capacity. Therefore, the pseudocapacitive behavior of porous $Zn_2Ti_3O_8$ highly promotes the actual capacity, which could provide ideas in designing other porous electrodes for lithium-ion batteries.

Declaration of competing interest

The authors declare that they have no known competing financial interests or personal relationships that could have appeared to influence the work reported in this paper.

Acknowledgments

The authors acknowledge the support of Project Supported by Keypoint Research and Invention in Shaanxi Province of China (No. 2020GY-270), Service local special plan project of Education Department of Shaanxi Province (No. 19JC009).

Supplementary materials

Supplementary material associated with this article can be found, in the online version, at doi:10.1016/j.cclet.2022.01.002.

References

[1] H. Li, Z. Wang, L. Chen, X. Huang, Adv. Mater. 21 (2009) 4593–4607.
[2] L. Lu, X. Han, J. Li, J. Hua, M. Ouyang, J. Power Sources 226 (2013) 272–288.
[3] H.H. Li, A. Saini, R.Y. Xu, et al., Rare Met 39 (2020) 1072–1081.
[4] V. Augustyn, P. Simon, B. Dunn, Energy Environ. Sci. 7 (2014) 1597.
[5] Y. Zhu, L. Peng, Z. Fang, et al., Adv. Mater. 30 (2018) e1706347.
[6] C. Huang, S.X. Zhao, H. Peng, et al., J. Mater. Chem. A 6 (2018) 14339–14351.
[7] J.H. Kim, K. Zhu, Y. Yan, C.L. Perkins, A.J. Frank, Nano Lett. 10 (2010) 4099–4104.
[8] V. Raju, J. Rains, C. Gates, et al., Nano Lett. 14 (2014) 4119–4124.
[9] L. Shen, E. Uchaker, X. Zhang, G. Cao, Adv. Mater. 24 (2012) 6502–6506.
[10] T. Yuan, Z. Tan, C. Ma, et al., Adv. Energy Mater. 7 (2017) 1601625.
[11] N. Wang, Z. Bai, Y. Qian, J. Yang, Adv. Mater. 28 (2016) 4126–4133.
[12] H. Tang, Z. Tang, C. Du, F. Qie, J. Zhu, Electrochim. Acta 120 (2014) 187–192.
[13] T.F. Yi, Y.R. Zhu, W. Tao, et al., J. Power Sources 399 (2018) 26–41.
[14] Z. Hong, M. Wei, Q. Deng, et al., Chem. Commun. 46 (2010) 740–742.
[15] W. Liao, J. Tian, Z. Shan, et al., Electrochim. Acta 216 (2016) 94–101.
[16] W. Liao, W. Li, J. Tian, et al., Electrochim. Acta 302 (2019) 363–372.
[17] J. Wang, J. Zhang, Y. Zhang, J. Guo, J. Zhang, J. Alloys Compd. 688 (2016) 392–398.
[18] X. Kong, X. Wang, D. Ma, et al., CrystEngComm 20 (2018) 7329–7336.
[19] D. Hu, X. Luo, X. Kong, et al., CrystEngComm 17 (2015) 1758–1764.
[20] C. Chen, L. Xu, G.A. Sewvandi, et al., Cryst. Growth Des. 14 (2014) 5801–5811.
[21] X. Kong, D. Hu, Y. Ishikawa, Y. Tanaka, Q. Feng, Chem. Mater. 23 (2011) 3978–3986.
[22] L. Wang, Y. Nie, X. Zhang, et al., Chem. Eng. J. 418 (2021) 129227.
[23] F. Borghi, C. Piazzoni, M. Ghidelli, P. Milani, A. Podestà, J. Phys. Chem. C 125 (2021) 1292–1303.
[24] S.J. An, J. Li, C. Daniel, et al., Carbon 105 (2016) 52–76.
[25] W. Chen, H. Liang, L. Shao, J. Shu, Z. Wang, Electrochim. Acta 152 (2015) 187–194.
[26] R. Hu, H. Zhang, Z. Lu, et al., Nano Energy 45 (2018) 255–265.
[27] I. Sultana, M.M. Rahman, Y. Chen, A.M. Glushenkov, Adv. Funct. Mater. 28 (2017) 1703857.
[28] F. Dinkelacker, P. Marzak, J. Yun, Y. Liang, A.S. Bandarenka, ACS Appl. Mater. Interfaces 10 (2018) 14063–14069.
[29] D.V. Safronov, S.A. Novikova, A.M. Skundin, A.B. Yaroslavtsev, Inorg. Mater. 48 (2011) 57–61.
[30] X. Wu, F. Kang, W. Duan, J. Li, Prog. Nat. Sci. Mater. 29 (2019) 247–255.
[31] J. Wu, Q. Yang, J. Li, et al., Electrochim. Acta 282 (2018) 30–37.
[32] Y. Li, F. Ma, L.W. Wang, J. Mater. Chem. A 6 (2018) 7815–7826.
[33] C. Pu, J. Yu, L. Fu, et al., Chin. Chem. Lett. 32 (2021) 1081–1085.
[34] P. Tan, Z. Wei, W. Shyy, T.S. Zhao, Appl. Energy 109 (2013) 275–282.
[35] Q. Li, H. Li, Q. Xia, et al., Nat. Mater. 20 (2021) 76–83.
[36] H. Liu, G. Zhang, X. Zheng, F. Chen, H. Duan, Int. J. Extrem. Manuf. 2 (2020) 042001.
[37] G. Zhang, J. Hu, Y. Nie, Y. Zhao, H. Duan, Adv. Funct. Mater. 31 (2021) 2100290.
[38] V. Augustyn, J. Come, M.A. Lowe, et al., Nat. Mater. 12 (2013) 518–522.
[39] G. Zhang, X. Zhang, H. Liu, et al., Adv. Energy Mater. 11 (2021) 2003927.
[40] B.H. Hou, Y.Y. Wang, J.Z. Guo, et al., ACS Appl. Mater. Interfaces 10 (2018) 3581–3589.
[41] D.S. Liu, D.H. Liu, B.H. Hou, et al., Electrochim. Acta 264 (2018) 292–300.
[42] J. Li, R. Wang, P. Guo, et al., ACS Nano 15 (2021) 6410–6419.
[43] S. Li, P. Xue, C. Lai, et al., Electrochim. Acta 180 (2015) 112–119.
[44] L. Zhang, X. Zhang, G. Tian, et al., Nat. Commun. 11 (2020) 3490.
[45] M. Lübke, P. Marchand, D.J.L. Brett, et al., J. Power Sources 305 (2016) 115–121.
[46] C. Lai, Y.Y. Dou, X. Li, X.P. Gao, J. Power Sources 195 (2010) 3676–3679.
[47] C. Wang, J. Huang, Y. Huang, et al., Carbon 169 (2020) 142–154.
[48] C. Wang, J. Huang, L. Cao, et al., Carbon 183 (2021) 899–911.
[49] X. Liu, T. Ji, H. Guo, et al., Electrochem. Energy Rev. 5 (2022) 401–433.